Supplementary Materials

Lateral, directional and polarized light emission from a silicon metasurface

Yuheng Mao[1#], Lidan Zhou[2#], Zhuo Wang[1], Shimei Liu[1], Fu Deng[1], Jinxiang Li[3], Jin Xiang[4], and Sheng Lan[1*]*

[1]Guangdong Provincial Key Laboratory of Nanophotonic Functional Materials and Devices School of Optoelectronic Science and Engineering, South China Normal University, Guangzhou 510006, P. R. China.

[2] State Key Laboratory of Optoelectronic Materials and Technologies, School of Electronics and Information Technology, Sun Yat-sen University, Guangzhou 510006, China.

[3]School of Electrical and Electronic Engineering, Nanyang Technological University, Singapore

[4]Key Laboratory of Optoelectronic Technology and Systems, Ministry of Education, and College of Optoelectronic Engineering, Chongqing University, Chongqing 400044, China.

[#]These authors contributed equally to this work.

[*]Corresponding author: jin@cqu.edu.cn (J. Xiang); slan@scnu.edu.cn (S. Lan)

Supplementary Note 1: Fabrication procedure of the silicon metasurfaces

In this work, we fabricated the silicon (Si) metasurfaces by using the combination of electron beam lithography and reactive ion etching. In Figure S1, we present the flowchart illustrating the fabrication process of the Si metasurfaces.

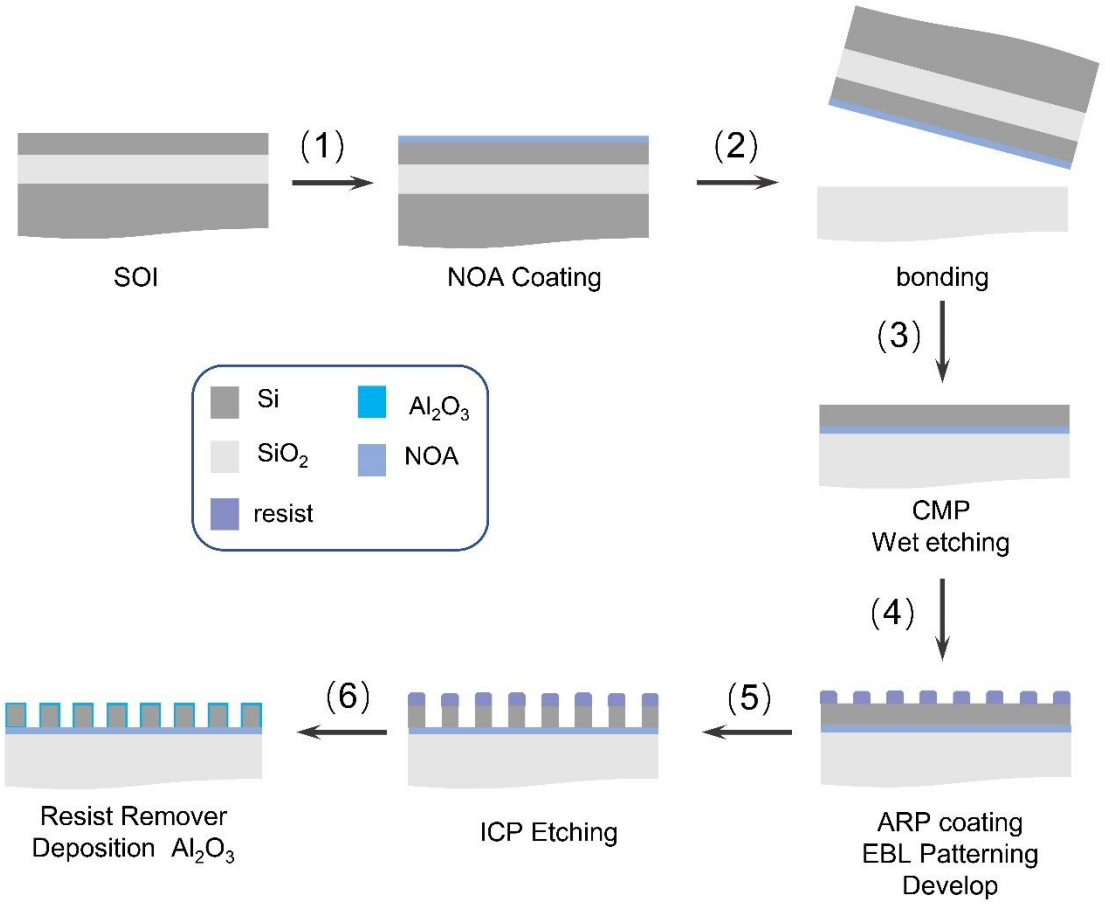

Figure S1. (1) Silicon-on-insulator (SOI) wafer (SOITEC) used for the fabrication of the Si metasurfaces. It consists of a 725-µm -thick undoped <100> Si substrate, a 2-µm-thick SiO_2 middle layer, and a 220-nm-thick crystalline-silicon (c-Si) top layer. An UV light curable adhesive (NOA61) was spin-coated on the sample. (2) The sample was bonded to a quartz substrate and illuminated by using 365-nm ultraviolet LED light to cross-link the adhesive for four hours. In order to achieve optimum adhesion, the sample was beforehand baked at 50°C for one day. (3) The Si substrate was then removed by chemical polishing and

wet etching. A c-Si on quartz substrate was obtained by removing the SiO_2 substrate of the SOI wafer with hydrofluoric (HF) acid. Partial c-Si top layer was etched and finally obtain a 130-nm-thick c-Si on quartz substrate. (4) A positive resist (ARP6200.09) was coated directly onto the c-Si at 4000 RPM for 60 seconds and baked on a hotplate at 180°C for 10 minutes. Then the pattern was exposed by using an electron-beam lithography system (EBPG5000Plus, Raith) operated at 100 kV. The resist was developed with xylene. (5) The pattern transfer was realized by using an inductively coupled plasma tool (Oxford Instruments). (7) The fabricated Si metasurfaces were covered with 5-nm-thick Al_2O_3 layer by using an atomic layer deposition system (SUNALE R-150, Picosun).

Supplementary Note 2: Influence of filleted corners in the Si nanocuboids on the reflection and transmission spectra of the Si metasurface

The reflection and transmission spectra of the Si metasurfaces placed on glass substrate were calculated by using the comercial software COMSOL. Based on the SEM images of the Si metasurfaces, it was found that the Si nanocuboids possess filleted corners rather than sharp corners. This feature was introduced inevitably in the fabrication process. In order to find out the influence of the filleted corners on the reflection and transmission spectra of the Si metasurface, we compared the reflection and transmission spectra of the Si metasurfaces composed of Si nanocuboids with sharp and filleted corners, as shown in Figures S2a and S2b. In the numerical simulations, a perfectly matched layer (PML) boundary condition was used in the *z* direction and a periodic boundary condition was used in the lateral directions (*x* and *y* directions). A *x*-polarized plane wave propagating along *z* direction irradiated on the unit cell. The refractive indices of Si was taken from Aspnes and Studna. It was found that the reflection (transmission) spectrum is shifted to a shorter wavelength while the spectral shape remains almost unchanged.

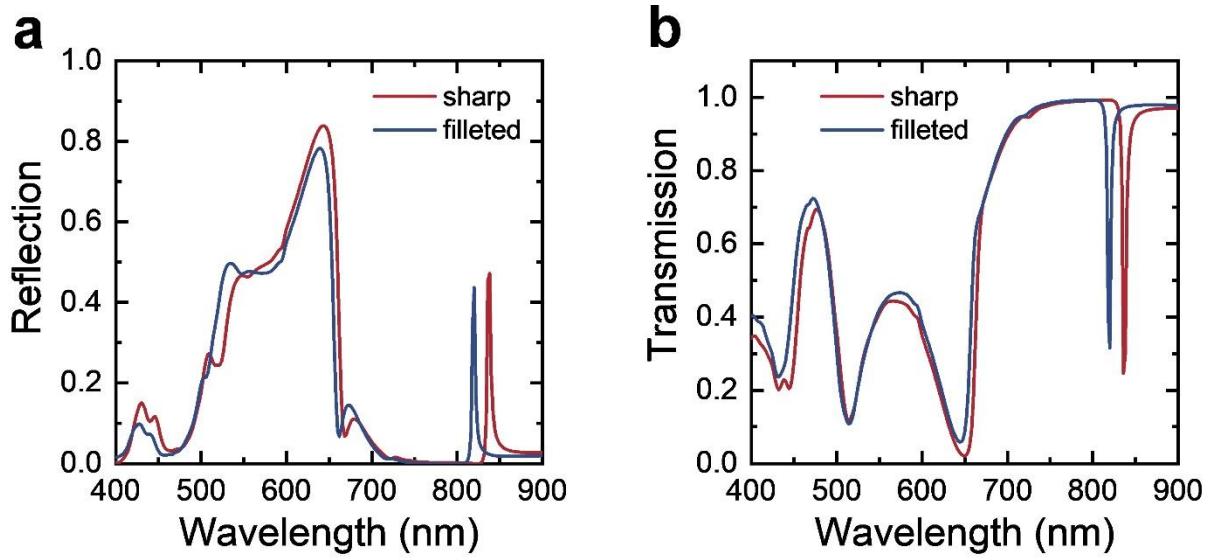

Figure S2. (a) Reflection and (b) transmission spectra calculated for the Si metasurfaces composed of Si nanocuboids with sharp and filleted corners.

Supplementary Note 3: Electric field and poynting vector distributions in the Si nanocuboids at the optical resonances of the Si metasurface

In Figures S3a–d, we show the electric field distributions in the *xy* plane calculated for mode A (λ = 819 nm), mode B (λ = 787 nm), mode C (λ = 650 nm) and mode D (λ = 510 nm). In Figures S3e and S3f, we also present the poynting vector distribution calculated for mode C and mode D. Additionally, we present the calculated angle-resolved reflection/transmission spectra of the Si metasurface, as shown in Figures S3g and S3h. In all cases, a plane wave polarized along the *x* direction was used to excite the Si metasurface (L = 250 nm). The bound states in the continuum (BIC) supported by the Si metasurface, which are denoted as A and B, are revealed in the spectrum. Mode A and mode B, which exhibit large angular dispersions, are identified as accidental BIC and symmetry-protected BIC, respectively. Since the accidental BIC (mode A) arising from the interference between EQ_{xy} and MD_z is expected to have large field enhancement and good radiation directionality, it is considered as a suitable cavity mode. Unfortunately, the two BICs appear in the near infrared spectral range where the radiative recombination rate of carriers is small. Thus, we failed to observe the enhanced luminescence from them in this study. A further reduction of the structural parameters is necessary in order to shift them to the visible light spectrum, which remains a big challenge in the fabrication of the Si metasurfaces.

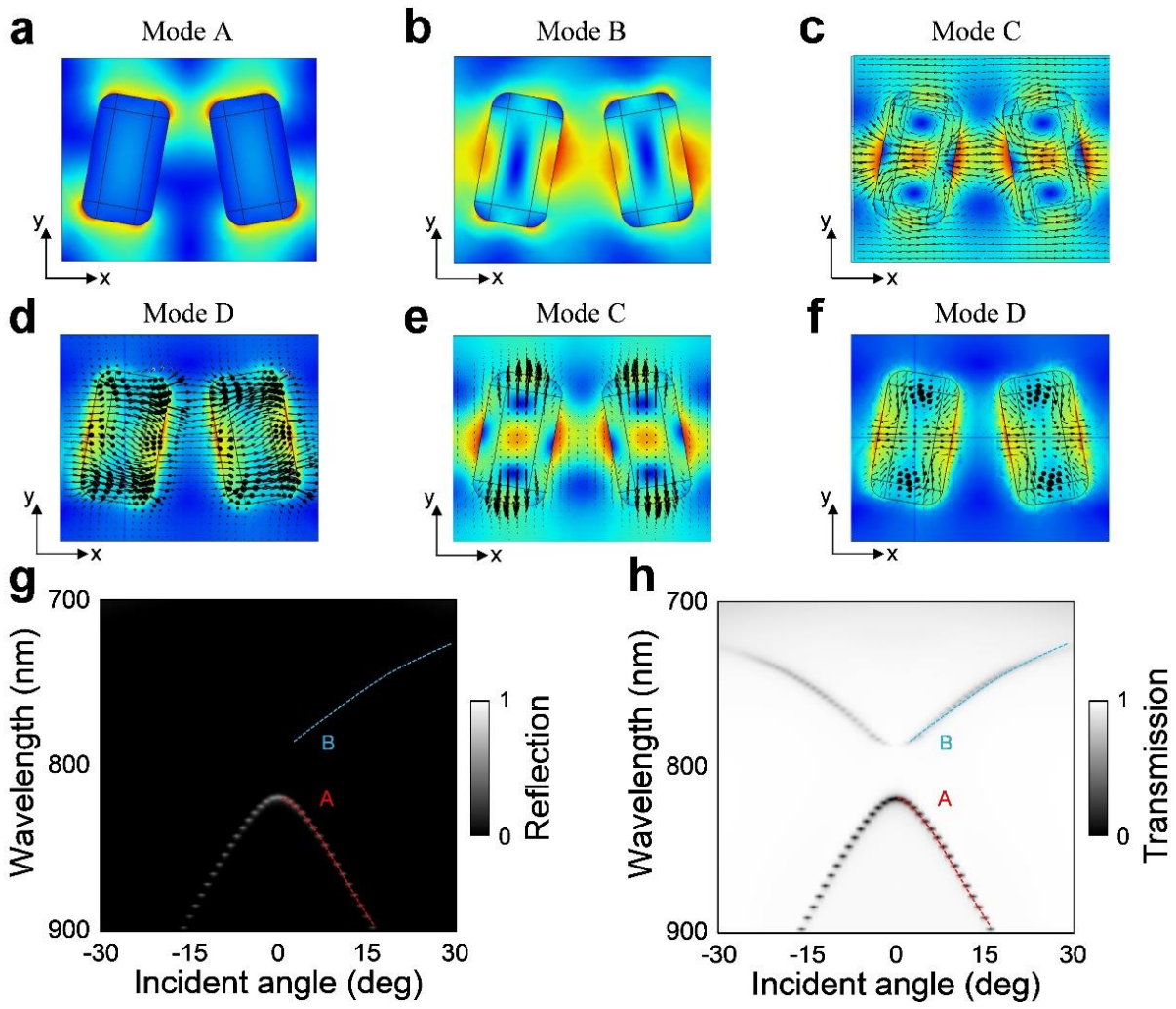

Figure S3. (a) and (b) Electric field distributions in the unit cell calculated for mode A (λ = 819 nm) and mode B (λ = 787 nm). (c) and (d) Electric field and vector distributions in the unit cell calculated for mode C (λ = 650 nm) and mode D (λ = 510 nm). (e) and (f) Electric field and poynting vector distributions in the unit cell calculated for mode C (λ = 650 nm) and mode D (λ = 510 nm). The angle-resolved reflection and transmission spectra calculated for the Si metasurface (L = 250 nm) are shown in (g) and (h), respectively.

Supplementary Note 4: Energy band analysis of the optical resonances

In Figure S4a, we present the energy band diagram calculated for the Si metasurface (L = 250 nm). and it can be observed a flat band in ~650 nm. Also, we calculated the angle-resolved transmission and reflection spectra for the Si metasurface, as shown in Figures S4b and S4c. In Figure S4d, we present angle-resolved reflection spectra measured for the Si metasurface (L = 250 nm). Although the signal-to-noise is not so good, one can still identify two flat bands at ~510 nm (mode D) and ~650 nm (mode C).

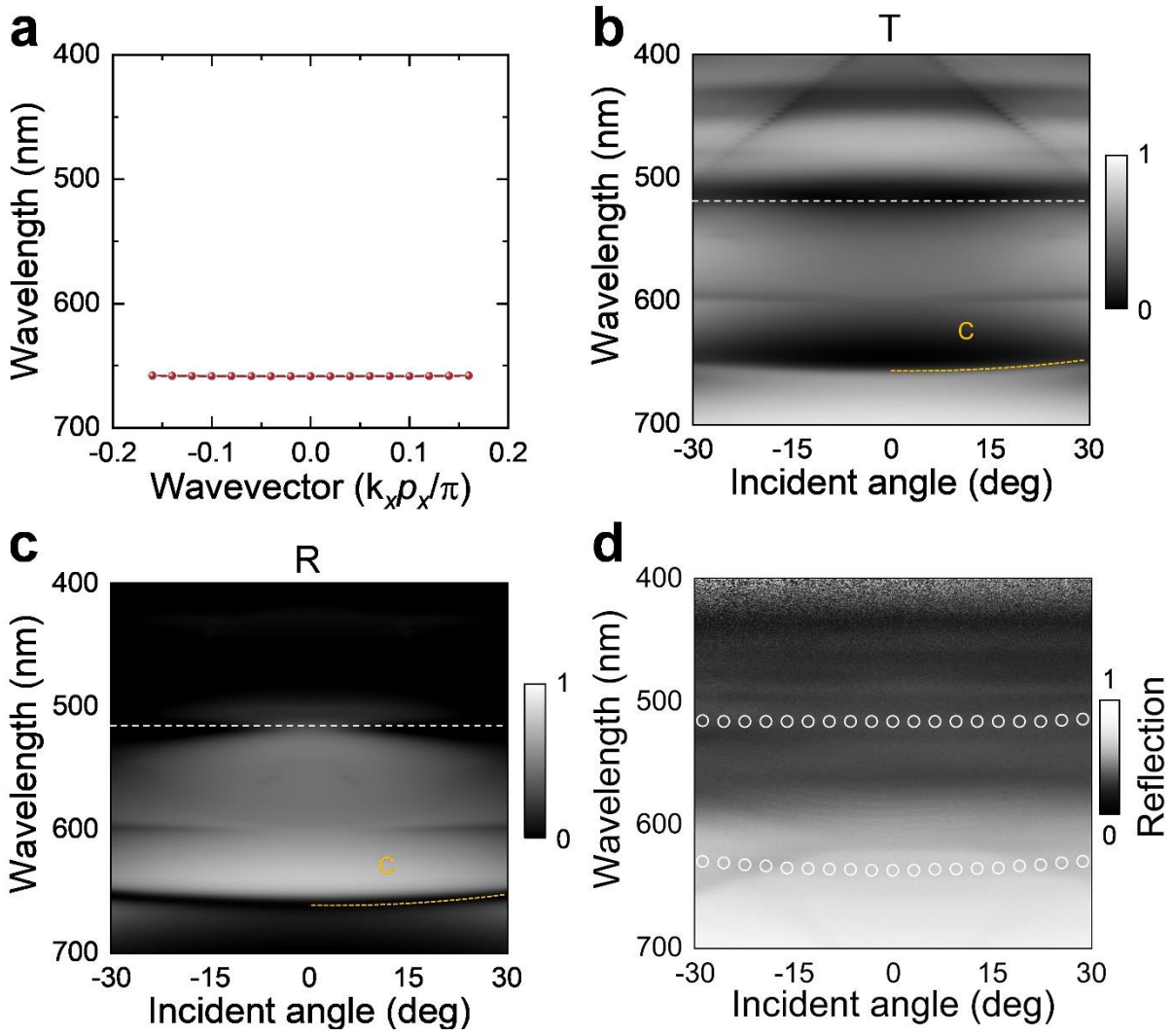

Figure S4. (a) Energy band diagram calculated for the Si metasurface (L = 250 nm). (b) Angle-resolved transmission spectra calculated for the Si metasurface (L = 250 nm). (c) Angle-resolved reflection spectra calculated for the Si metasurface (L = 250 nm). (d) Angle-resolved reflection spectra measured for the Si metasurface (L = 250 nm).

Supplementary Note 5: Analysis of the scattering spectrum of the unit cell and the reflection spectrum of the metasurface

In order to find out the physical origins for the optical resonances appearing in the scattering spectrum of the unit cell (paired Si nanocuboids) and the reflection spectrum of the Si metasurface, we employed the multipolar expansion method to analyze the scattering spectrum of the unit cell and the reflection spectrum of the Si metasurface. The results are shown in Figure S5. In the numerical calculations, we examined the contributions of electric dipole (ED), magnetic dipole (MD), electric quadrupole (EQ), magnetic quadrupole (MQ) by using the following formulas[1]:

$$ED = \frac{1}{i\omega}\int \boldsymbol{J} d^3\boldsymbol{r}, \tag{1}$$

$$TD = \frac{1}{10c}\int [(\boldsymbol{r}\cdot\boldsymbol{J})\boldsymbol{r} - 2(\boldsymbol{r}\cdot\boldsymbol{r})J] d^3\boldsymbol{r}, \tag{2}$$

$$MD = \frac{1}{2c}\int (\boldsymbol{r}\times\boldsymbol{J}) d^3\boldsymbol{r}, \tag{3}$$

$$EQ_{\alpha\beta} = \frac{1}{i2\omega}\int [\boldsymbol{r}_\alpha \boldsymbol{J}_\beta + \boldsymbol{r}_\beta \boldsymbol{J}_\alpha - \frac{2}{3}(\boldsymbol{r}\cdot\boldsymbol{J})\delta_{\alpha\beta}] d^3\boldsymbol{r}, \tag{4}$$

$$MQ_{\alpha\beta} = \frac{1}{3c}\int [(\boldsymbol{r}\times\boldsymbol{J})_\alpha \boldsymbol{r}_\beta + (\boldsymbol{r}\times\boldsymbol{J})_\beta \boldsymbol{r}_\alpha] d^3\boldsymbol{r}, \tag{5}$$

where c is the speed of light in vacuum, and α, β represent the Cartesian coordinate components x, y, z. The current density $\boldsymbol{J}$ is derived from the electric field inside the nanocuboids by $-\mathrm{i}\omega\varepsilon_0[\varepsilon_r(\boldsymbol{r}) - \varepsilon_{r,d}]\boldsymbol{E}(\boldsymbol{r})$. The radiated power of each multipole was calculated as follows[1],

$$I_p = \frac{2\omega^4}{3c^3}|\vec{p}|^2, I_m = \frac{2\omega^4}{3c^3}|\vec{m}|^2, I_T = \frac{2\omega^6}{3c^5}\left|\vec{T}\right|^2,$$
$$I_{EQ_{\alpha\beta}} = \frac{\omega^6}{5c^5}\left|\overrightarrow{EQ}_{\alpha\beta}\right|^2, I_{MQ_{\alpha\beta}} = \frac{\omega^6}{40c^5}\left|\overrightarrow{MQ}_{\alpha\beta}\right|^2. \tag{6}$$

In the calculation of the scattering spectrum of the unit cell, the PML boundary condition was applied in the x, y, z directions. In the calculation of the reflection spectrum of the metasurface,

the PML boundary condition was used in the *z* direction and a periodic boundary condition was employed in the *x* and *y* directions.

As shown in the Figures S5a and S5b, the MQ_{yz} in the metasurface is narrower than that in the single unit cell. This behavior indicates the coupling between unit cells, which leads to the lateral energy transfer along the *y* direction.

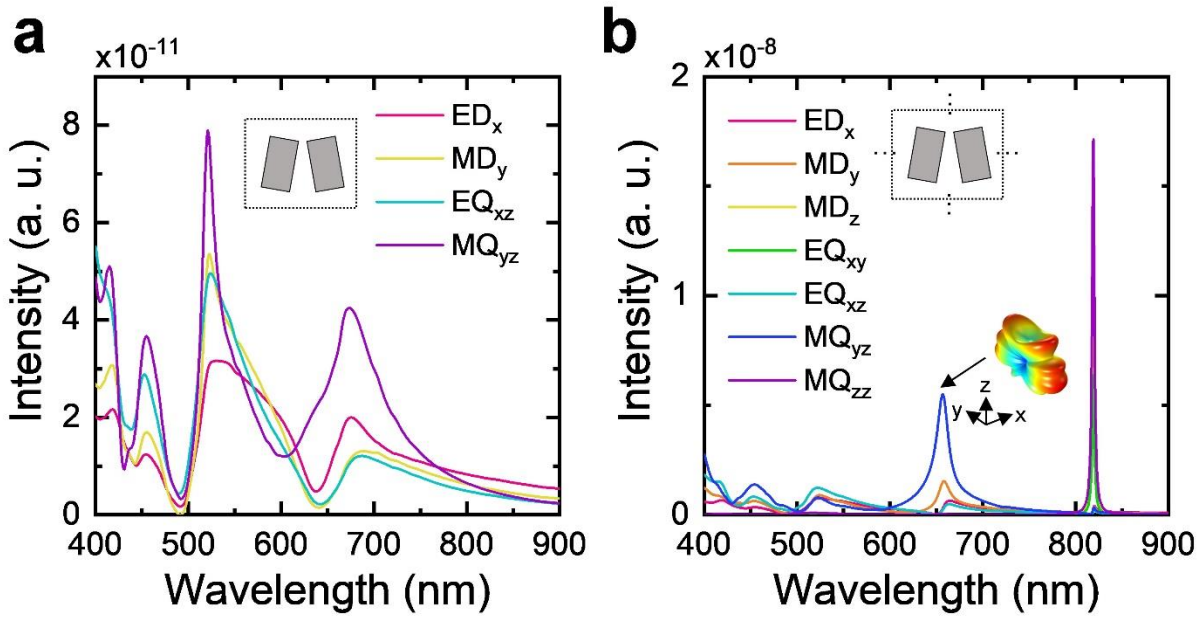

Figure S5. Multipolar expansion of the scattering spectrum of the unit cell (a) and the reflection spectrum of the metasurface (b).

Supplementary Note 6: Calculation of the radiative properties of the Si metasurface

In Figure S6a, we randomly deployed 50 electric dipoles in the two Si nanocuboids and examined the radiative properties of the Si metasurface by using the commercial software (COMSOL). A detector placed above the Si metasurface was used to collect the power flow propagating along z direction. The radiative power was derived from the surface-integrated power flow. In Figure S6b, we present the Purcell factor of the Si metasurface, which is determined by the ratio of radiated power with and without the Si metasurface. The calculated emission spectrum is provided in Figure S6c for comparison.

In a previous study, the influence of the carrier density injected into a Si nanoparticle on the dielectric constant of Si was investigated.[2] Based on this study, we derived the refractive indices of Si at different carrier densities and used them to calculate the emission spectra of the Si metasurface at different optical doping levels, as shown in Figure S6d. And the emission spectra of the Si metasurfaces was simulated by using the COMSOL.

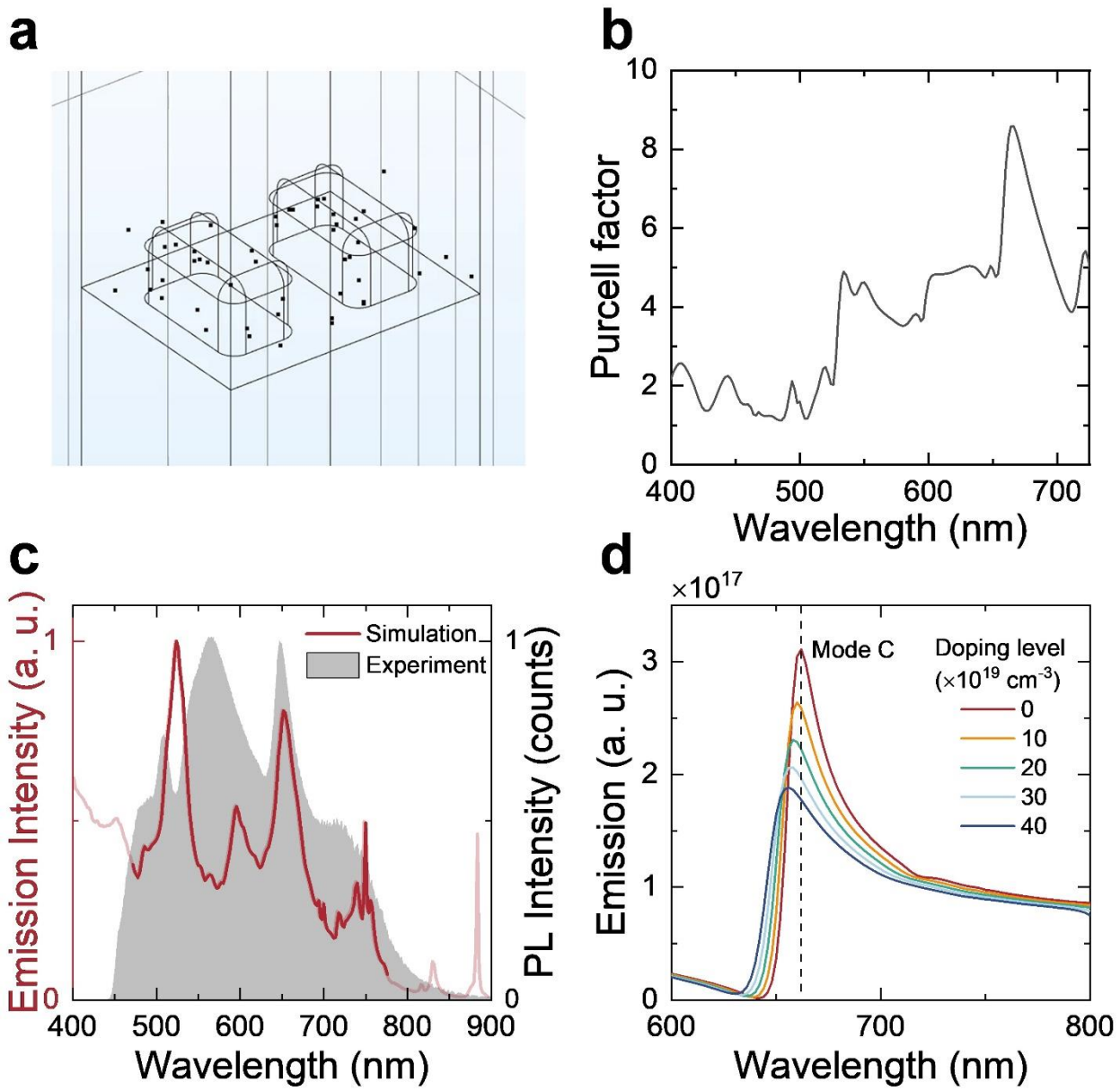

Figure S6. (a) Numerical model used to calculate the emission spectrum of the Si metasurface. (b) Calculated Purcell factor of the Si metasurface (L = 250 nm). (c) Calculated emission spectrum of the Si metasurface (L = 250 nm) and the measured PL spectrum is also provided. (d) Emission spectra of the Si metasurface at different optical doping levels.

Supplementary Note 7: Reflection spectra of the Si metasurfaces obtained by using the cross-polarization method

In Figure S7, we show schematically the experimental setup used to measure the reflection spectra of the Si metasurfaces by using the cross-polarization method. The white light is polarized by using a polarizer and focused on the Si metasurface with a 4× objective. The reflected light from the Si metasurface is collected by using the same objective and directed to a spectrometer for analysis and a CCD for imaging. A polarizer with its transmission axis perpendicular to that of the polarizer (used to polarize the white light) is inserted into the collection channel. In this way, the optical resonances supported by the Si metasurface can be revealed in the reflection spectrum.

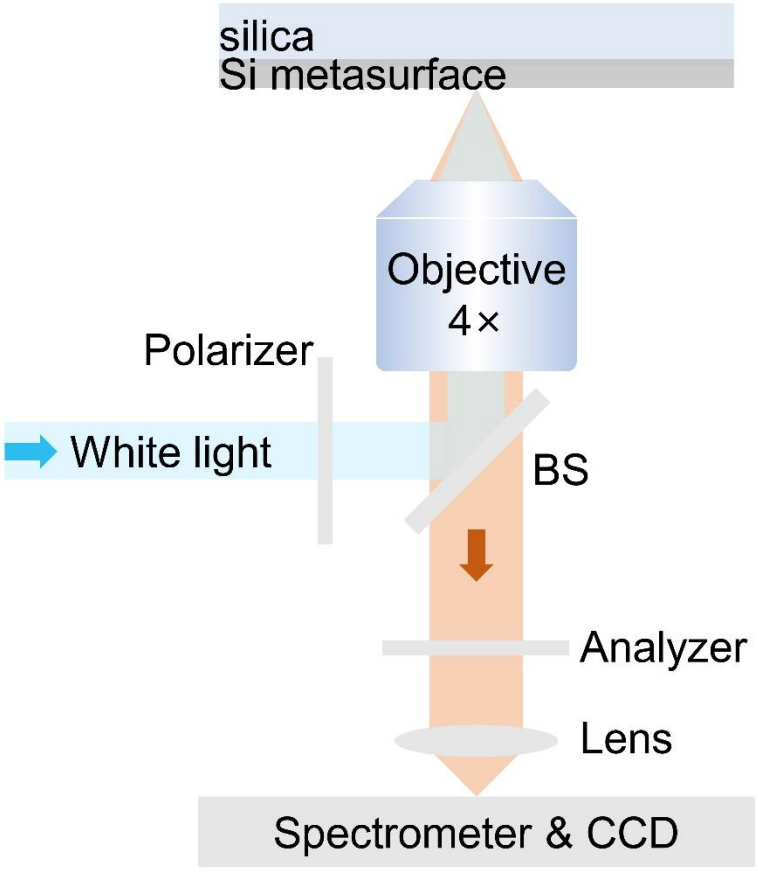

Figure S7. Experimental setup used to measure the reflection spectra of the Si metasurfaces.

Supplementary Note 8: Carrier dynamics in a Si nanoparticle excited by 400-nm femtosecond laser light and 325-nm continuous wave laser light

In Figure S8, we show schematically the carrier dynamics in Si nanoparticles or metasurfaces excited by using 400-nm femtosecond laser pulses and 325-nm continuous wave (CW) laser light. Since the bandgap of Si at the Γ point is ~3.4 eV, the transition of electrons from the valence band to the conduction band can be achieved via direct transition, two-photon-induced absorption (TPA), and indirect transition assisted by phonons. As a result, high-density hot electrons can be generated at the bottom of the conduction band. Meanwhile, the high temperature in Si nanoparticles induced by the thermalization of hot electrons may trigger the intrinsic excitation of carriers, which continuously supplies electrons from the valence band to the Δ point of the conduction band. Enhanced by the high-density electrons at the Δ point, the Auger effect continuously lifts the carriers from low-energy states to high-energy states. As a result, the hot electrons can stay at the Γ point for a sufficiently enlarged relaxation time. On the other hand, the radiative recombination assisted by phonons can be accelerated by optical resonances, leading to an enhanced photoluminescence (PL). The combination of these effects leads to the white-light emission from Si nanoparticles or Si metasurfaces.

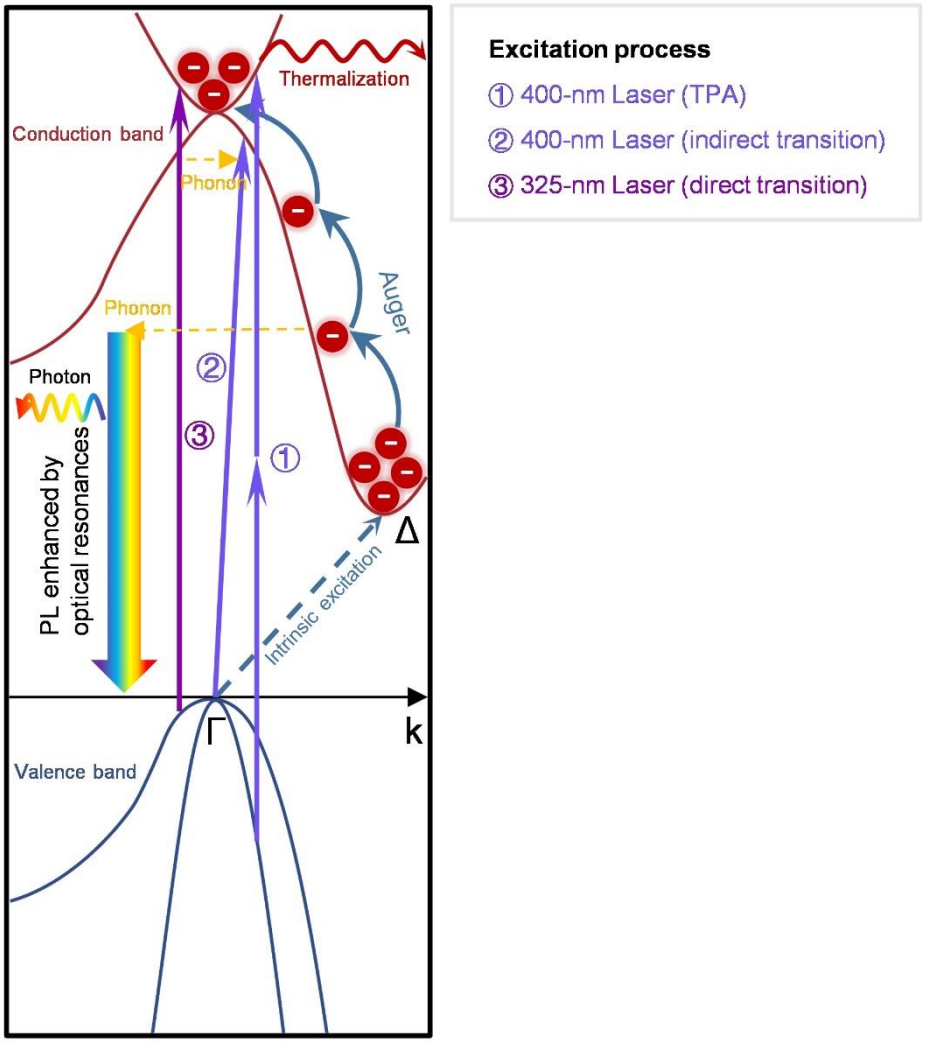

Figure S8. Carrier dynamics in Si nanoparticles/metasurfaces excited by using 400-nm femtosecond laser pulses and 325-nm continuous wave laser light.

Supplementary Note 9: Fitting of the PL spectra with multiple Lorentz lineshapes

In Figure S9, we show the fitting of a typical PL spectrum with multiple Lorentz lineshapes. In this way, the linewidths and integrated intensities of the PL peaks observed in the PL spectrum can be extracted.

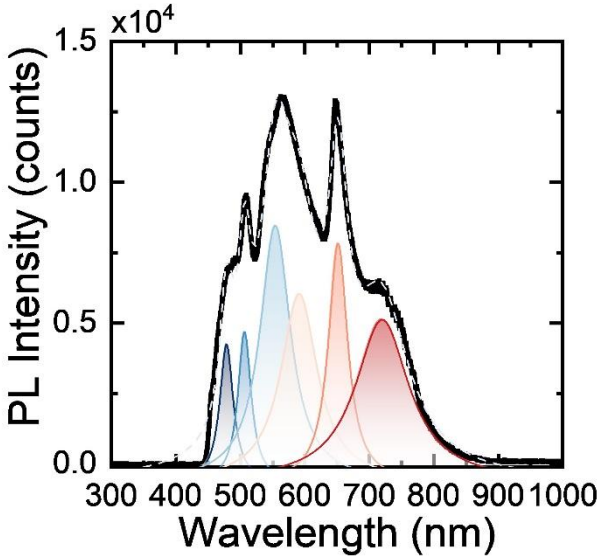

Figure S9. Fitting of the PL spectrum with multiple Lorentz lineshapes.

Supplementary Note 10: Experimental setup used for characterizing the light emission and propagation in the Si metasurfaces

The linear and nonlinear optical properties of Si metasurfaces were characterized by using an inverted microscope (Observer A1, Zeiss) equipped with white light and femtosecond laser light as excitation sources.

For the characterization of nonlinear optical responses, we used 400-nm femtosecond laser pulses delivered by a Second Harmonic Generation System (Coherent), which was pumped by 800-nm femtosecond laser pulses with a duration of 130 fs and a repetition rate of 76 MHz (Mira HP, Coherent), to excite Si metasurfaces. The excitation light was focused on Si metasurfaces by using a 10× objective of the microscope and the hot electron luminescence emitted from Si metasurfaces were collected by using the same objective and directed to a spectrometer (SR-500i-B1, Andor) for spectral analysis or to a charge-coupled device (DU970N, Andor) for imaging. The diameter of laser spot was estimated to be ~10 μm ($1/e^2$). In Figures S10a, S10b and S10c, we present the PL spectra obtained at the laser spot, the propagating route of the luminescence in the *x* direction, and the propagating route of the luminescence scattered by a defect in the *y* direction. It was found that the luminescence propagating in the *x* direction is dominated by the blue-green light while that propagating in the *y* direction is dominated by the yellow-red light. The CCD image of the Si metasurface under the excitation of laser light is shown in Figure S10d.

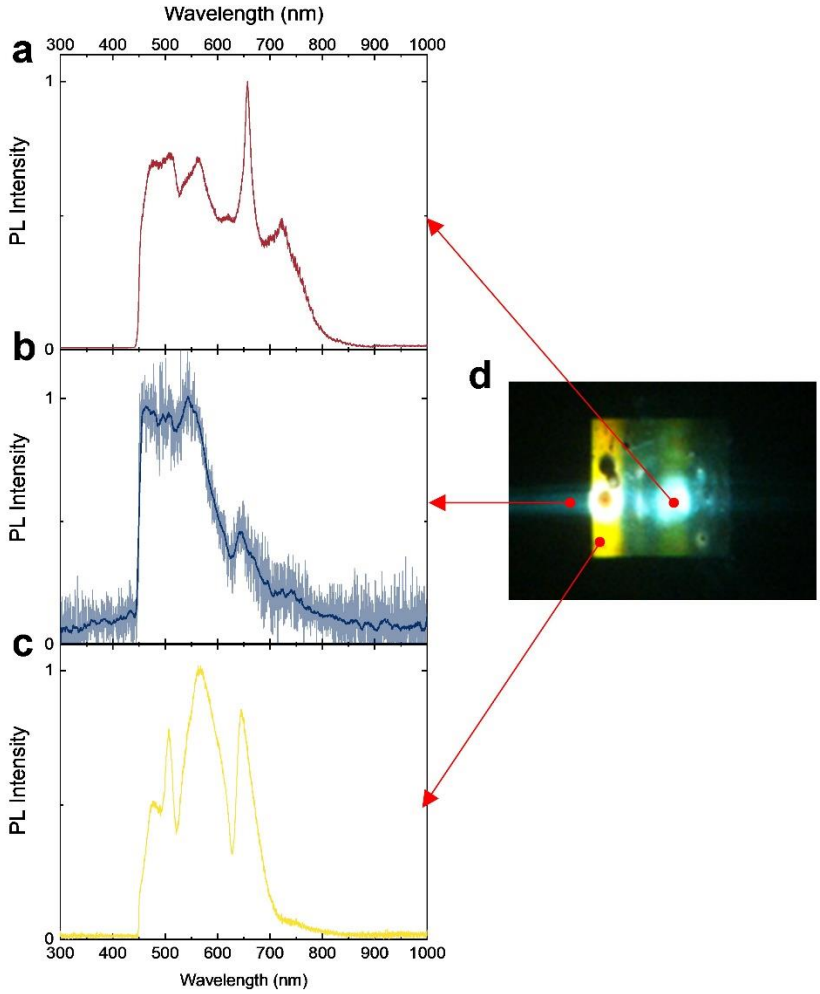

Figure S10. PL spectra measured at different locations. (a) At the laser spot. (b) At the propagating route of the luminescence in the *x* direction. (c) At the propagating route of the luminescence scattered by a defect in the *y* direction. (d) CCD image of the Si metasurface under the excitation of the laser light.

Supplementary Note 11: PL spectra measured with different rotation angles of the sample

In Figure S11, we present the PL spectra measured with different rotation angles of the sample. It can be seen that varying the rotation angle has little effect on either the spectral profile or relative intensity of the green and yellow light emission.

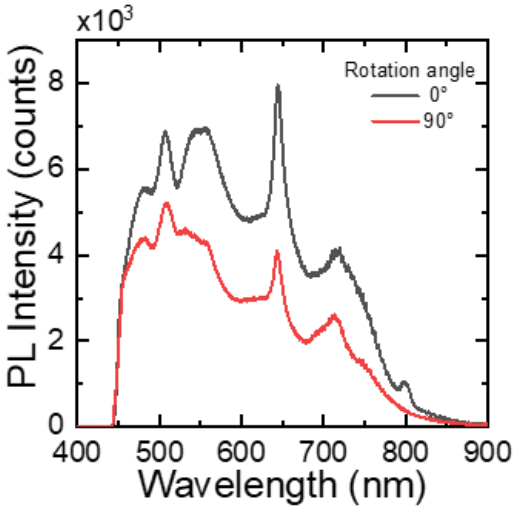

Figure S11. PL spectra measured with different rotation angles of the sample.

Supplementary Note 12: Polarization characterization of the light emission from the Si metasurface

We measured the PL spectra of the Si metasurface (L = 250 nm) by using a polarization analyzer with different polarization angles, as shown in Figure S12a. The dependence of the luminescence intensity on the polarization angle measured for mode D and mode C are shown in Figure S12b and S12c. In both cases, one can see linearly polarized luminescence along the y direction. However, mode C exhibits a higher degree of polarization as compared with mode D.

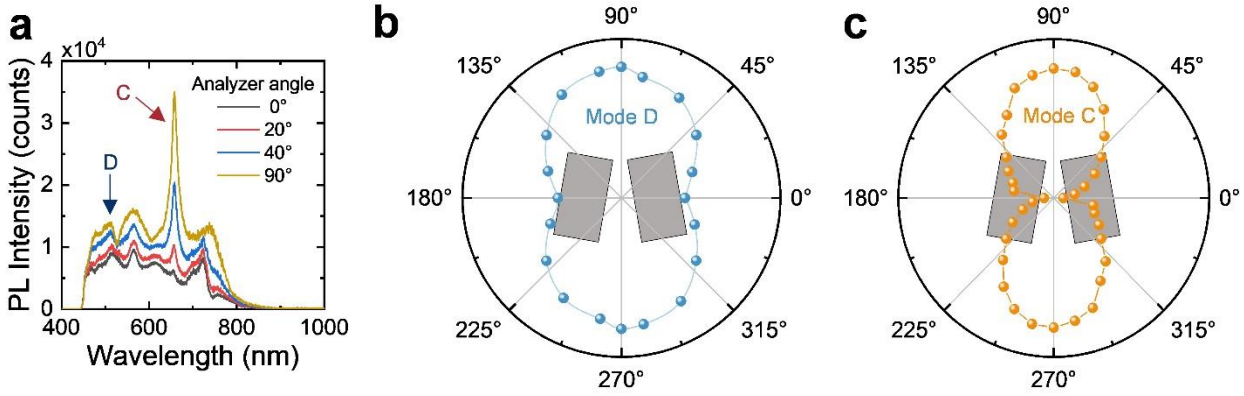

Figure S12. (a) PL spectra measured for the Si metasurface (L = 250 nm) by using a polarization analyzer with different angles. (b) Dependence of the luminescence intensity on the polarization angle measured for mode D. (c) Dependence of the luminescence intensity on the polarization angle measured for mode C.

Supplementary Note 13: Morphologies of the Si metasurfaces and the "defect" induced by using photothermal effect

In Figure S13, we examined the morphologies of the metasurfaces and the "defect" induced by using photothermal effect by using scanning electron microscopy (SEM) (Ultra 55, Zeiss). In Figures S13a, b, we present the SEM images of two different metasurfaces. In Figure S13c, we also show the top view of the Si metasurfaces of all parameters. By applying photothermal effect, we introduced "defect" into the Si metasurfaces, as shown in Figures S13d, e, f. It can be seen that the "defect" is a surface elevation and the Si nanocuboids maintain a good shape.

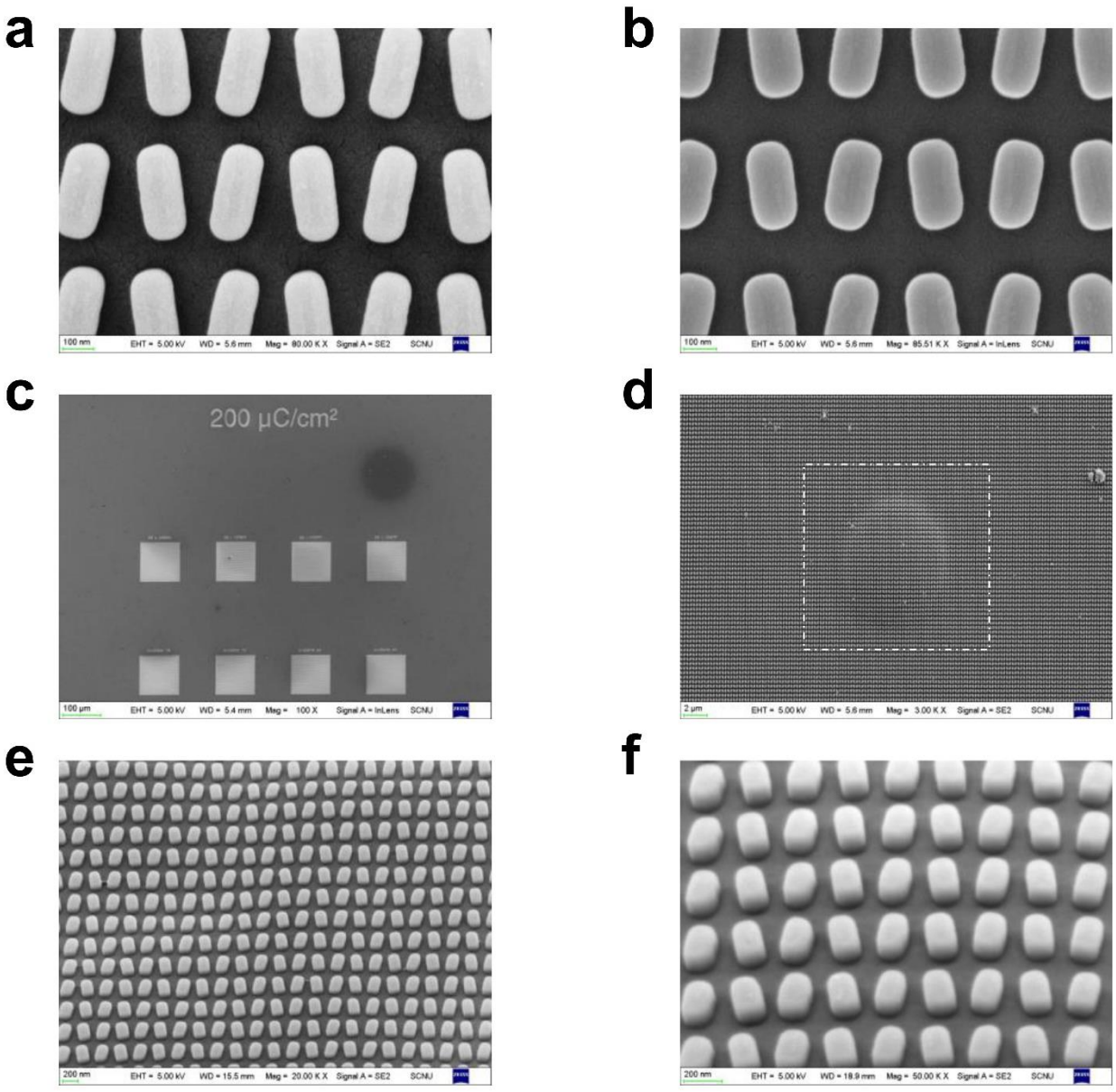

Figure S13. (a)(b) SEM images of two different Si metasurfaces. (c) The top view of the Si metasurfaces of all parameters. (d)−(f) SEM images of the "defect" induced by using photothermal effect.

Reference

(1) Zhou, C.; Li, S.; Wang, Y.; Zhan, M. Multiple Toroidal Dipole Fano Resonances of Asymmetric Dielectric Nanohole Arrays. *Phys. Rev. B* **2019**, *100*, 195306.

(2) Xiang, J.; Chen, J.; Dai, Q.; Tie, S.; Lan, S.; Miroshnichenko, A. E. Modifying Mie Resonances and Carrier Dynamics of Silicon Nanoparticles by Dense Electron-Hole Plasmas. *Phys. Rev. Appl.* **2020**, *13*, 014003.